ScientificScholar®
Knowledge is power
Publisher of Scientific Journals

https://arabjchem.org

Arabian Journal of Chemistry

Article in Press

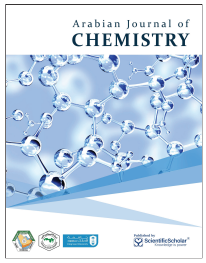

Original Article

Aryl diazonium-mediated functionalization of mesoporous silica nanoparticles with acid blue 193 for efficient dispersed solid-phase extraction of trace Chromium (III) from environmental samples

Awadh Owyimer AlSuhaimi*

Department of Chemistry, Faculty of Science, Taibah University, Medina Munwarah, Saudi Arabia

ARTICLE INFO

Keywords:
Aryldiazonium chemistry
Acid blue 193
Chromium
dSPE
ICPMS
Mesoporous silica nanoparticles
Surface functionalisation

ABSTRACT

Aryl diazonium chemistry provides a robust and versatile route for covalent surface functionalization. It allows a controlled introduction of functional groups for advanced analytical and separation applications. In this work, the strategy was applied to graft Acid blue 193 (AB193) onto mesoporous silica nanoparticles (MSNs). The MSNs were synthesized from a sodium silicate precursor using a simple room-temperature sol–gel method, providing an ecofriendly route to porous silica nanoparticles. The resulted stable hybrid nanochelator (MSNs-AB193) was applied as a dispersed solid-phase extraction (dSPE) nanosorbent for the preconcentration of chromium(III) from aqueous samples. Structural and spectroscopic characterizations using Fourier transform infrared spectroscopy (FTIR), elemental analysis, thermogravimetric analysis (TGA), scanning electron microscopy (SEM), and brunauer–emmett–teller (BET), confirmed the successfulness of surface modification. Adsorption experiments demonstrated a pronounced pH-dependent uptake of Cr(III), achieving a maximum adsorption capacity of approximately 68 mg g^{-1} at pH 5. Equilibrium was rapidly reached within 30 min, and the adsorption kinetics were best described by a pseudo-second-order model. The Langmuir isotherm indicated that the sorption process was dominated by chemisorption. Nearly quantitative recovery (>99%) was achieved using 1.0 M HNO_3 as an eluent. The MSNs-AB193 dSPE method, when coupled with inductively coupled plasma mass spectrometry (ICP-MS) detection, provided an effective and reliable sample-preparation strategy for the determination of Cr(III) in water matrices. The method exhibited excellent analytical characteristics, including wide linearity (R^2 = 0.998), high sensitivity (LOD = 0.007 $\mu g \cdot L^{-1}$), and good precision (RSD = 1.73% at 5 $\mu g \cdot L^{-1}$). Its accuracy was confirmed through the analysis of ions in EnviroMAT™ groundwater certified reference materials, which produced recoveries of 93–95%. The method was applied to determine chromium concentrations in real groundwater samples from Al-Madinah Al-Munawarah, Saudi Arabia. The measured concentrations ranged from 15 to 17 $\mu g \cdot L^{-1}$, which are within the World Health Organization (WHO) guideline limits. The sorbent further demonstrated notable chemical stability under acidic to mildly alkaline conditions and retained its extraction performance after more than 10 months of storage.

1. Introduction

Solid-phase extraction (SPE) has been established as a fundamental sample-preparation technique, particularly for the determination of trace analytes such as heavy metals *from complex matrices*. It enables selective isolation and effective pre-concentration of target species from interfering constituents, thereby it enhances analytical sensitivity and accuracy [1]. Crucially, the effectiveness of this method hinges largely on the sorbent material, as its chemical selectivity, adsorption capacity, and kinetic properties directly dictate both extraction performance and the reliability of subsequent instrumental quantification. Over the last few years, nanomaterials have transformed this field, especially when used in dSPE mode. Their remarkably high surface-to-volume ratio and abundance of readily accessible active sites result in significantly faster mass-transfer rates and adsorption kinetics compared to conventional bulk sorbents. In addition, their surfaces can be precisely tailored through covalent functionalization, polymer coating, or specific ligand immobilization, providing exquisite control over metal-ion selectivity [2]. Within the exist diverse family of nanostructured sorbents, silica nanoparticles (SNPs)—particularly mesoporous silica nanoparticles (MSNs)—have attracted considerable attention because of their high surface areas, ordered pore networks, and abundant surface silanol groups that enable facile modification [3]. Moreover, MSNs can be prepared from renewable and sustainable precursors, such as the abundant sodium silicate or bio-silica obtained from agricultural wastes including rice husk ash and sugarcane bagasse, which lowers cost and promotes eco-friendly nanomaterial production [4,5].

Despite their favorable physicochemical characteristics, bare (unmodified) silica nanoparticles generally display low intrinsic selectivity toward metal ions, which limits their direct applicability in analytical extraction and sensing. Post-synthesis surface functionalization is a widely adopted strategy to overcome this

***Corresponding author:**
E-mail address: asuhaimi@taibahu.edu.sa (A. O. AlSuhaimi)

Received: 02 September, 2025 **Accepted:** 29 December, 2025 **Epub Ahead of Print:** 05 March, 2026 **Published:** ***
DOI: 10.25259/AJC_1051_2025

limitation, with silanization being the most versatile approach. Organosilanes such as 3-aminopropyltriethoxysilane (APTES) and 3-mercaptopropyltrimethoxysilane introduce amino (–NH_2) and thiol (–SH) groups onto the silica surface, providing weak chelating sites for metal-ion coordination [6,7]. Beyond the introduction of chelating functionalities, silanization serves as a versatile surface-engineering strategy that provides reactive anchoring motifs for the covalent immobilization of selective ligands, thereby significantly expanding the functional design space of silica-based materials. Silane-derived reactive centers enable precisely controlled post-grafting chemistries, most notably amide bond formation with carboxyl-containing chelators, yielding chemically robust and interfacially stable architectures. Moreover, a wide range of reactive silane functionalities, including amine, thiol, epoxide (glycidyl), and isocyanate groups, further broadens chelator attachment pathways via nucleophilic epoxide ring-opening reactions or amide/urethane linkage formation [8], nucleophilic substitution with halogenated ligands [9], and Schiff-base condensation with aldehyde-functionalized chelators [10]. Furthermore, advanced functionalization routes—such as click reactions and atom transfer radical polymerization (ATRP)—enable controlled grafting of complex ligand frameworks [11], thereby offering enhanced versatility and tunability in sorbent design. Nevertheless, silanization still faces critical limitations, notably hydrolytic instability of the siloxane bonds, steric restrictions that can impede full surface coverage, and batch-to-batch variability that compromises reproducibility [12,13].

These challenges motivate the development of more robust immobilization strategies capable of ensuring stable ligand attachment and consistent material performance. Aryl diazonium salt chemistry, first introduced for the modification of carbon, metals, and semiconductor surfaces [14], provides a robust and versatile alternative to classical salinization for tailoring silica interfaces. In this strategy, aryl diazonium salts are generated in situ—typically via diazotization of the corresponding anilines—and subsequently reduced to produce highly reactive aryl radicals. These radicals undergo covalent attachment to surface silanol groups, forming stable C–O and C–Si linkages that are markedly more resistant to hydrolysis and thermal degradation than conventional siloxane-based bonds [15,16].

Compared with silane grafting, diazonium-mediated functionalization typically achieves higher grafting densities, superior reproducibility, and enhanced long-term stability owing to the robustness of the radical-driven coupling process [15,16]. The methodological versatility is well demonstrated across diverse applications, including the incorporation of diazonium-modified silica into polymeric composites [16] and the construction of silica–iron oxide nanohybrids with improved interfacial stability [15]. Recent comprehensive reviews have further highlighted the broad utility of aryl diazonium chemistry in modifying fillers, oxides, and in particular silica, underscoring its increasing relevance as a dependable alternative to silane chemistry [17,18].

Despite its extensive use as a surface-modification tool, the application of aryldiazonium chemistry specifically for constructing metal-chelating materials remains very limited. To date, only the reported studies from our group have demonstrated its use for preparing chelated carbon and polymeric substrates [19,20], underscoring that no work has yet extended this methodology to silica surfaces. This absence highlights a clear gap in the development of selective inorganic sorbents based on aryldiazonium grafting.

In this study, we address this gap by presenting the first aryldiazonium-grafted mesoporous silica chelator, prepared through the immobilization of the Cr(III)-selective azo dye Acid Blue 193 (AB193). AB193 forms highly stable 1:2 Cr(III) complexes and is available commercially only in its Cr(III) form, underscoring its intrinsic affinity for this metal [21]. Further enhancement of selectivity within multifaceted sample matrices is accomplished via the strategic implementation of a thiourea-mediated masking regimen, which proficiently sequesters interfering transition metal ions without compromising the coordinative accessibility of Cr(III) [22].

This combined strategy yields an MSN–AB193 hybrid that functions as a selective, matrix-tolerant dSPE sorbent for Cr(III) across diverse water samples.

2. Materials and Methods

2.1. Chemicals and materials

All reagents used in the synthesis, functionalisation of MSNs, and throughout the analytical procedures were of analytical grade and used without further purifications. Sodium silicate solution ($Na_2O{\cdot}3SiO_2$; Na_2O: 8%, SiO_2: 27%) was a gift from Adwan Chemical Industries Co. Ltd. (Riyadh, KSA). Polysorbate Tween 80 was sourced from HEG Chemical Co., Ltd. (Hefei Anhui, China), while Triton X-100, 4-nitrobenzene diazonium tetrafluoroborate (NBDT), hypophosphorous acid, and ascorbic acid were obtained from Sigma-Aldrich Chemie GmbH (Darmstadt, Germany). Ammonium acetate, thiourea masking agent and sodium hydrosulfite ($Na_2S_2O_4$) were purchased from Panreac (Barcelona, Spain), nitric acid from Loba Chemie (Mumbai, India), and ammonium hydroxide solution from Sigma Aldrich (Seelze, Germany). Standard metal ion stock solutions (1000 mg/L) and Acid Blue 193 dye were provided by Acros Organics (Geel, Belgium). Solution pH was adjusted using ammonium acetate buffer or nitric acid as needed. Aqueous solutions in all experiments prepared in ultrapure water (Milli-Q® Type 1, Merck KGaA, Darmstadt, Germany). Glassware was cleaned with Mobi detergent (Nafco, Riyadh), soaked in 5% HNO_3 for 24 h, and rinsed with ultrapure water before use.

2.2. Apparatus and instrumentations

Attenuated total reflectance–fourier transform infrared (ATR–FTIR) spectra were collected on a Thermo Scientific FT-IR spectrometer with a diamond ATR accessory (Waltham, MA, USA) to verify surface chemistry of the chelator. thermogravimetric analysis (TGA) was performed on a NEXTA STA200 simultaneous thermogravimetric analysis/differential scanning calorimetry (TGA/DSC) analyzer (Hitachi High-Tech, Tokyo, Japan) to quantify organic loading and assess thermal stability of resin. Particle morphology was examined by field-emission scanning electron microscopy (SEM) (ZEISS, Oberkochen, Germany) after Pt coating. Nanoparticle size distribution and mean particle size were determined from SEM micrographs using ImageJ 1.54g (National Institutes of Health, Bethesda, MD, USA). Nitrogen adsorption–desorption isotherms at −195.8°C were acquired on a Micromeritics ASAP 2020 analyzer (Norcross, GA, USA) to obtain brunauer–emmett–teller (BET) surface area and pore-size distributions ($4V/S_{BET}$; BJH/NLDFT). Total metal concentrations were determined by inductively coupled plasma–mass spectrometry (ICP-MS) (7500 series, Agilent Technologies, Santa Clara, CA, USA).

2.3. Preparation of Mesoporous silica nanoparticles

MSNs were synthesized via a room temperature sol–gel method from sodium silicate solution as the silica precursor, following a procedure developed in our laboratory [23]. Briefly, a sodium silicate solution (50 mL, 5% w/v) was added dropwise under continuous stirring to a homogeneous mixture containing 50 mL of ethanol, 50 mL of water, 2 g of ascorbic acid (serving as both a pH adjuster and a catalytic agent), 0.20 mL of Triton X-100, and 0.25 mL of polysorbate 80. The resulting mixture was stirred at ambient temperature for 45 min. to promote hydrolysis and condensation, then aged 24 h at room temperature. The product was separated by centrifugation (4000 rpm, 10 min), washed several times with water and ethanol, dried at 80°C for 4 h, and finally calcined at 550°C. This process yielded MSNs with well-controlled porosity and morphology.

2.4. Functionalization of MSNs with acid blue

MSNs were chemically functionalized with Acid Blue 193 (AB193) dye via a stepwise aryl diazonium strategy designed to anchor aryl-amino groups, which were subsequently reduced and utilized in a diazo-coupling reaction. Briefly, 5 g of MSNs was first reacted with 30 mM 4-NBDT under vigorous stirring, followed by the dropwise addition of hypophosphorous acid at 5°C for 30 min to yield nitro-functionalized MSNs (MSN–NO_2). The resulting solid was collected by centrifugation, washed sequentially with water and acetonitrile, and dried the vacuum.

The nitro groups were then reduced using 5% sodium hydrosulfite at 45°C for 24 h, affording aminated MSNs (MSN–NH_2). After isolation, the aminated particles were subjected to diazotization with 2% sodium nitrite in 1% acetic acid at 0–5°C for 1.5 h, then centrifuged, washed and redispersed in a 10 mL cold ethanol. Immediately thereafter, a 1% ethanolic solution of AB193 dye was added to the suspension to carry out the diazo-coupling step. The final product (MSN–AB193) was thoroughly washed with ethanol, deionized water, and 2% HCl until the washings became colorless, then vacuum-dried and stored in a desiccator.

2.5. Adsorption study

Batch adsorption experiments were conducted to evaluate the influence of pH, contact time, sorption capacity, isothermal behavior, and adsorption kinetics. Complete reduction of Cr(VI) to Cr(III) was achieved by adding 5 mL of ascorbic acid solution (5 mM) and allowing the mixture to agitate for 5–10 min [10]. After the reduction step, the solution pH was adjusted to the desired value, followed by the addition of 100 mg of MSNs–AB193 into 100 mL of Cr(III) solution. The suspension was then agitated for predetermined intervals, and aliquots were withdrawn, separated, and analyzed. Adsorption data were fitted using the Langmuir isotherm to determine maximum sorption capacity, while the pseudo-second order (PSO) kinetic model was applied to elucidate the adsorption mechanism.

2.6. dSPE process

dSPE was performed using the AB193–MSN nanosorbent. A known mass of the sorbent was conditioned with deionized water and dispersed into 25 mL of standard Cr(III) solutions, certified waters, or wastewater samples [10]. To minimize interference from Fe(III), Al(III), Mn(II), Cu(II), and other transition metals, thiourea was added to each sample to achieve a final concentration of 0.05 mol L^{-1}, selectively complexing competing ions while leaving Cr(III) available for extraction. After a 3–5 min equilibration period, the solution pH was adjusted to 5.0, the optimized condition that maintains Cr(III) in its cationic hydroxo–aqua form and promotes selective interaction with the AB193 functional groups on the MSN surface. The suspension was agitated for 5 min and centrifuged to isolate the Cr(III)-loaded nanosorbent. The separated solid was then re-dispersed in 2.5 mL HNO_3 (0.25–2.5 M) to elute the bound Cr(III). The eluates were diluted with deionized water and analyzed by ICP-MS. Calibration was performed using synthetic groundwater [24] and method performance was validated with EnviroMAT™ CRMs (ES-L-1, Analytichem, Canada).

3. Results and Discussion

3.1. Synthesis and characterization of MSN-AB193

The MSNs used as substrates for AB193 immobilization were synthesized using a room-temperature sol–gel method previously developed by our group [23]. The resulting particles exhibited a uniform spherical morphology and a well-ordered mesoporous structure, providing a robust platform for high-density ligand grafting. The chemical immobilization of the AB193 chelating ligand onto the MSNs was achieved via an aryl-diazonium-mediated grafting strategy that ensures a densely packed, covalently robust, and hydrolytically stable surface layer. Initially, 4-NBDT was grafted onto the silica surface through reductive activation using hypophosphorous acid, a well-established reagent for converting diazonium salts into reactive aryl radicals. On silica surfaces, two complementary grafting mechanisms operate simultaneously. The primary pathway involves reductive homolysis of the diazonium salt to generate aryl radicals (Ar·), which directly attack surface silicon atoms to form strong Si–C bonds [16,25]. Concurrently, the low isoelectric point of silica (pH ~2–3) promotes partial deprotonation of surface silanol groups (Si–OH → SiO^-) even under mildly acidic conditions. These negatively charged SiO^- sites electrostatically attract diazonium cations ($SiO^-\cdots{}^+N_2$–Ar), enabling an interfacial grafting route that may proceed via transient diazo-ether intermediates (Si–O–N=N–Ar) or heterolytic dediazoniation. Subsequent mild thermal curing (~110°C) converts these adducts into stable Si–O–aryl linkages [16,17]. This dual radical/interfacial mechanism is typical of diazonium chemistry on silica and related metal oxides such as TiO_2 and ZrO_2 [25].

The nitro groups on the grafted aryl layer were then selectively reduced to primary amines, which were covalently coupled to the chromophoric AB193 ligand [19,20]. The resulting material presents a highly accessible and chemically stable chelating interface with strong affinity and selectivity for Cr(III), consistent with previous reports on aminated diazonium-functionalized sorbents [20]. Successful functionalization at each stage was readily confirmed by distinct color changes: white for pristine MSNs, yellow orange after nitroaryl grafting, and deep brown red upon final AB193 immobilization (Figure 1).

The structural and chemical characteristics of MSNs–AB193 were confirmed by ATR–FTIR, TGA, CHNS, SEM–EDX, and BET/BJH analyses.

3.1.1. ATR-FTIR analysis

ATR–FTIR spectra (Figure S1) provided detailed insight into the chemical changes occurring at the MSN surface during functionalization. The pristine MSNs displayed the typical siloxane framework bands at ~1080, 805, and 460 cm^{-1}, consistent with the formation of a robust silica network [26]. Following diazonium grafting and azo-coupling, several new diagnostic absorptions appeared, including aromatic C=C stretches (1600–1450 cm^{-1}), azo (–N=N–) bands, and sulfonate vibrations (1180–1030 cm^{-1}) originating from the AB193 chromophore. These features confirm that the functional groups responsible for metal chelation were successfully and covalently anchored onto the silica surface. Importantly, the retention of the Si–O–Si bands indicates that the core mesostructure remained intact throughout the multi-step chemical modification. The overall spectral profile strongly suggests that AB193 is immobilized through stable covalent linkages rather than weak physisorption [12,13].

3.1.2. Thermogravimetric analysis

Thermogravimetric analysis (Figure S2) provided quantitative confirmation of the organic loading introduced onto the MSNs. Pristine MSNs exhibited only minor mass loss up to 800°C, attributable mainly to desorption of physically bound water. In contrast, MSNs–AB193 showed a pronounced multi-step decomposition pattern between 200–550°C, corresponding to the sequential breakdown of aryl layers, azo linkages, and the AB193 chromophore. The total organic mass fraction of approximately 17% aligns with values reported for diazonium-modified silica surfaces [15,16], indicating efficient surface coverage. The gradual decomposition profile also points to strong covalent anchoring rather than loosely bound or unreacted organic species. The lack of abrupt mass-loss events further implies that the underlying silica matrix remains thermally stable post-functionalization [27].

3.1.3. Elemental (CHNS) composition

CHNS analysis (Table 1) provided additional confirmation of successful grafting [28]. The experimentally derived C:S and N:S mass % ratios (22.3:1 and 4.81:1, respectively) closely matched the theoretical stoichiometry of the immobilized AB193 moiety (approximated as $C_{22}N_4S_1$ from Figure 1). This result is critical, as it indicates not only the presence of sulfur (from the sulfonate group) and nitrogen (from azo and amine groups), but also their proportionality relative to carbon — a hallmark of successful and complete azo-coupling reactions. The agreement between theoretical and experimental values supports the

Table 1. Comparison of theoretical and experimental C:N:S ratios for MSN–AB193.

Ratio	Theoretical ($C_{22}N_4S_1$)	Sample 4 (CHNS)
C : N	5.50 : 1	4.83 : 1
C : S	22.0 : 1	22.3 : 1
N : S	4.0 : 1	4.81 : 1

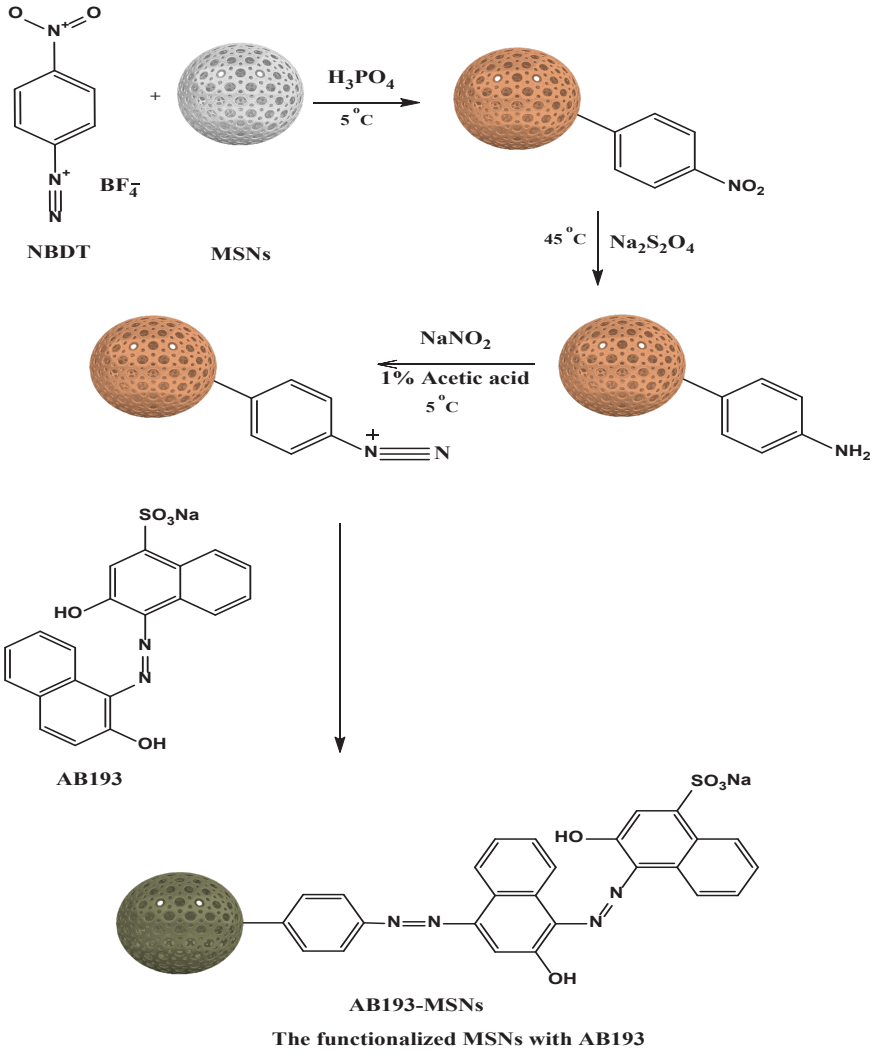

Figure 1. Schematic of MSNs-AB193 synthesis via aryl diazonium grafting. 4-NBDT is reduced by H_3PO_2 to aryl radicals, which covalently bind to pristine MSNs forming stable Si–C linkages. Subsequent coupling with Acid blue 193 yields the final hybrid material (MSNs-AB193).
Color progression: white (pristine MSNs) → pale orange (diazonium-grafted MSNs) → dark brown (MSNs-AB193).

conclusion that AB193 molecules are uniformly distributed across the MSN surface, rather than forming isolated or incomplete surface patches.

3.1.4. Textural properties (BET surface area and porosity)

The SEM micrographs together with particle size histograms (Figure 2) highlight the morphological and size evolution of MSNs before and after modification. Plain MSNs show uniform spherical particles with smooth surfaces, narrow size distribution, and an average particle size of ~220 nm, consistent with sol–gel synthesized mesoporous silica [28,29]. (Figure 2a) MSNs-AB193, while retaining the spherical morphology, exhibit rougher surfaces, slight aggregation, and a broader distribution with an increased average size of ~250 nm. These changes confirm that AB193 functionalization modifies surface properties and promotes modest growth in particle size due to clustering, in line with earlier reports on dye-functionalized mesoporous silica.

Nitrogen adsorption–desorption isotherms (Figure 2b) of plain MSNs exhibited a typical type-IV profile with a sharp capillary condensation step, confirming mesoporosity. BET analysis showed a high surface area (~756 m^2/g), pore diameter (~8 nm), and pore volume (~1.6 cm^3/g). After AB193 loading, these values decreased markedly (~315 m^2/g, ~6.2 nm, ~1.2 cm^3/g), indicating partial pore blocking and dye incorporation. The shifted isotherm further supports reduced pore accessibility [29].

3.2. Sorption models and optimization

A systematic evaluation of pH influence, adsorption kinetics, equilibrium isotherms and eluent strength was conducted to elucidate the interaction characteristics of Cr(III) with MSNs–AB193 and to establish the operational parameters required for efficient dSPE. The combined dataset presented in Figures 3-6 and Table 2 enable a unified interpretation of the uptake–release behavior governing the analytical performance of the functionalized mesoporous silica.

3.2.1. Effect of pH on Cr(III) uptake

The effect of pH on Cr(III) adsorption is shown in Figure 3. Adsorption increases markedly from acidic conditions to pH 5, where the maximum loading (~68 mg g^{-1}) is achieved. This trend reflects the interplay between ligand protonation and metal speciation: at low pH, protonation of the azo and phenolic groups on AB193 suppresses metal coordination, while increasing pH promotes ligand deprotonation and facilitates chelation. Beyond pH 6, a decline in uptake is observed, attributed to the onset of $Cr(OH)_3$ precipitation, which reduces the availability of soluble species for surface binding. These results are consistent with the behavior previously reported for dye-functionalized silica systems [30].

A comparison of sorption capacities (Table 2) highlights the enhanced performance of MSNs–AB193, which outperforms AB193-

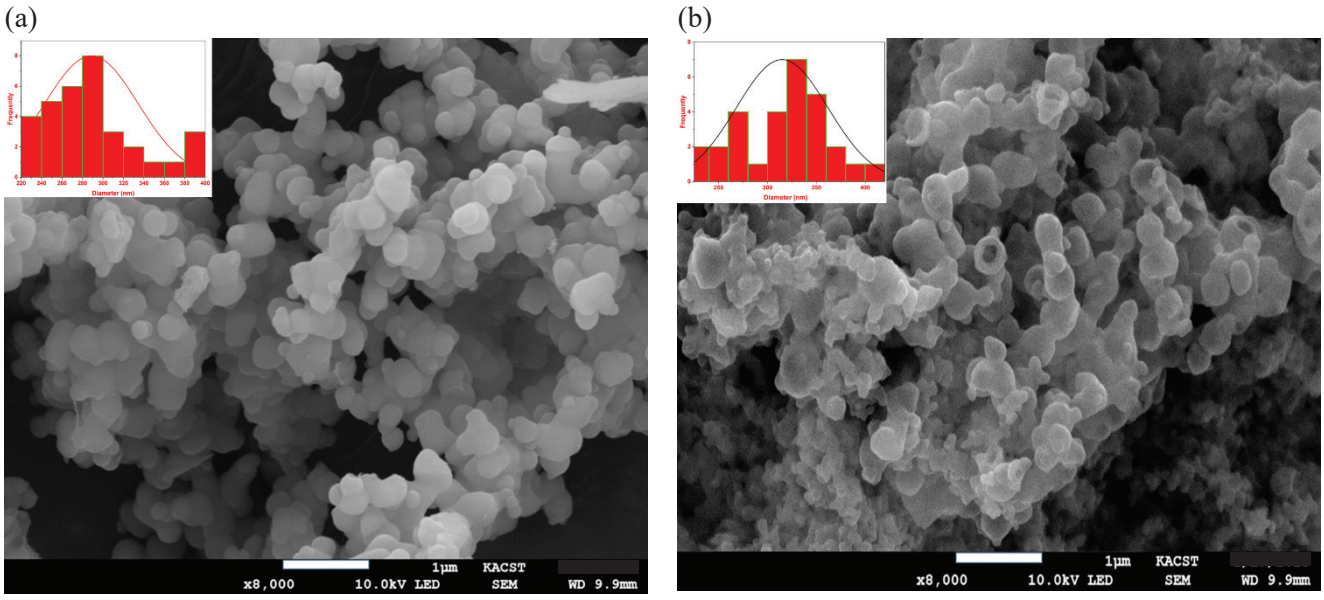

Figure 2. SEM micrographs of (a) plain MSNs and (b) MSNs-AB193, with particle size distributions shown in the insets. Plain MSNs exhibit an average particle size of ~220 nm, while MSNs-AB193 show a larger average size of ~250 nm with rougher surface morphology and slight aggregation after surface modification.

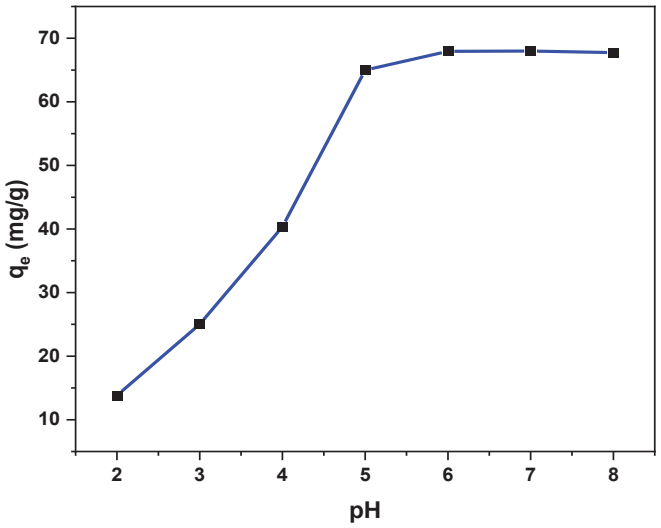

Figure 3. Effect of solution pH on Cr(III) sorption capacity (qe) by MSNs–AB193. Uptake increases with pH, reaching maximum binding (~68 mg/g) at pH 5–6 due to coordination via azo (–N=N–) and phenolic –OH groups of Acid blue 193.

immobilised polymeric resins such as XAD-4 (20.9 mg g^{-1}) [1 and XAD-2 (3.35 mg g^{-1}) [31]. The 3–20-fold rise in capacity emphasizes the advantage of using mesoporous silica nanoparticles in providing a high density of accessible, uniformly distributed chelating sites.

3.2.2. Adsorption kinetics and rate-controlling mechanisms

The kinetic data in Figure 4(a) were analyzed using the pseudo-first order (PFO), pseudo-second order (PSO), and intraparticle diffusion (IPD) models. The models are computed from equations (1)-(3):

$$\text{Pseudo-first-order (PFO)}: \ln\left(q_e - q_t\right) = \ln q_e - k_1 t \quad (1)$$

$$\text{Pseudo-second-order (PSO)}: \frac{t}{q_t} = \frac{1}{k_2 q_e^2} + \frac{t}{q_e} \quad (2)$$

$$\text{Intraparticle diffusion (IPD)}: q_t = k_{id} t^{\frac{1}{2}} + C \quad (3)$$

Where q_e & q_t: Adsorbed amounts at equilibrium and time t. K_2, k_id, C: Rate constants for chemisorption, pore diffusion, and boundary layer thickness.

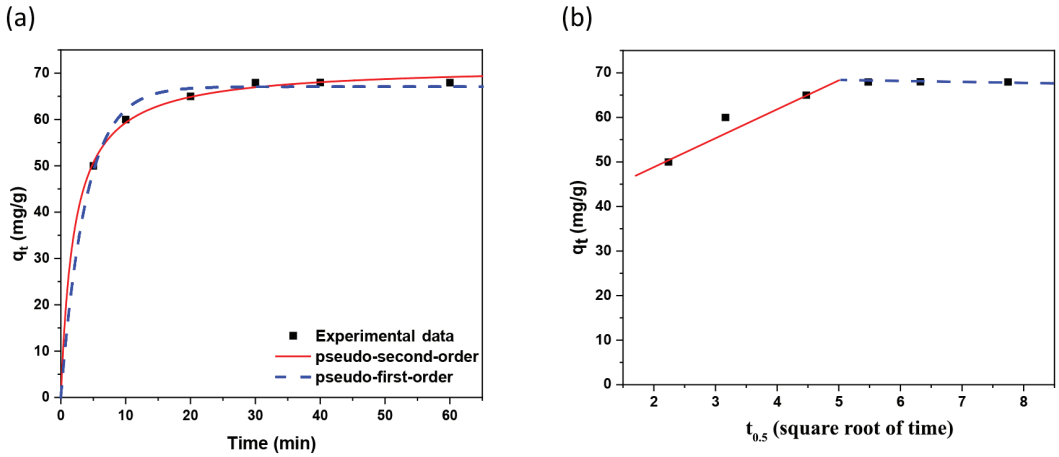

Figure 4. (a) PFO and PSO kinetic fits. (b) Weber–Morris IPD model. Key parameters: PFO (K1 = 0.26, qe = 68.4 mg g^{-1}, R^2 = 0.94); PSO (K2 = 0.00677, qe = 70.6 mg g^{-1}, R^2 = 0.98); IPD Stage I (Kid = 6.61, C = 36.9, R^2 = 0.93); Stage II (Kid = 0.0055, qe ≈ 68 mg g^{-1}, R^2 = 0.91).

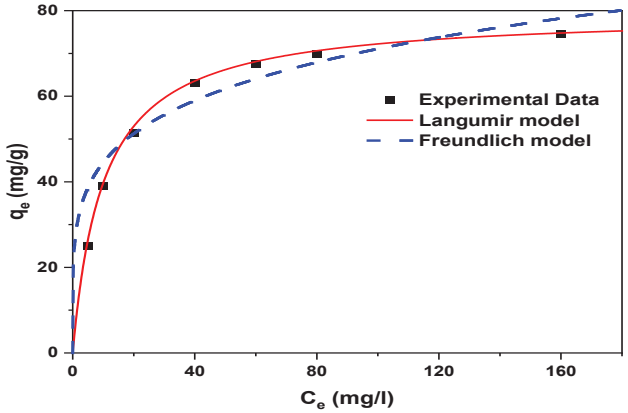

Figure 5. Adsorption isotherms for Cr(III) on AB193-MSNs. Langmuir: qmax = 68.4 mgg^{-1}, KL = 0.1, R^2 = 0.998; Freundlich: KF = 27.9, n = 4.9, R^2 = 0.89.

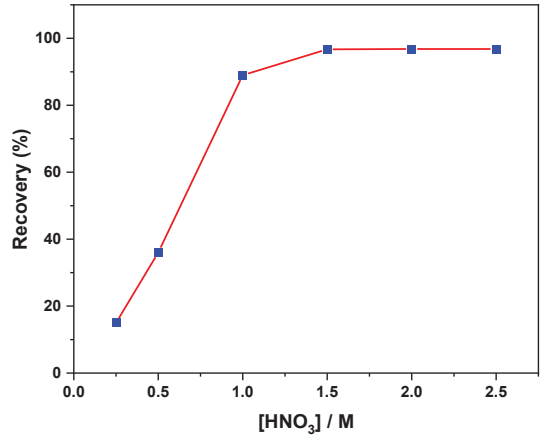

Figure 6. Effect of HNO_3 eluent concentration on Cr (III) desorption from MSNs-AB193 (25 mg resin, 25 mL eluent).

Table 2. Comparison of sorption capacities (SC) (mg g^{-1}) of Acid blue 193 immobilized on different substrates and other adsorbents for Cr(III).

Substrate	SC (mg/g)	LOD (μgL^{-1})	RSD (%)	Reference
MSNs-AB193	68	0.007	2.34	This work
Amberlite XAD-4-AB193	20.9			[31]
Amberlite XAD-2-AB193	3.35			[32]

The PSO model exhibited the best agreement with experimental data (R^2 = 0.987), with calculated qe values closely matching those obtained experimentally, indicating that the adsorption process is governed predominantly by chemisorption at AB193 functional groups. The PFO model provided an inferior fit, confirming that physical adsorption is not the dominant mechanism. The IPD plot shown in Figure 4(b) reveals two linear regions, corresponding to an initial surface-controlled diffusion step followed by slower intraparticle diffusion. The non-zero intercept (C ≠ 0) indicates that intraparticle diffusion is not the sole rate-controlling mechanism, consistent with behavior reported for silica-based mesoporous adsorbents [4,13]. An equilibration time of 30 min is therefore sufficient for attaining adsorption equilibrium under the optimized conditions.

3.2.3. Equilibrium isotherms and surface energetics

The equilibrium sorption data were analyzed by fitting to the linearized forms of the Langmuir and Freundlich isotherm models, as described by Equations (4) and (5).

$$\text{Langmuir isotherm}: \frac{C_e}{q_e} = \frac{1}{K_L q_{\max}} + \frac{C_e}{q_{\max}} \quad (4)$$

$$\text{Freundlich isotherm}: \ln q_e = \ln K_F + \frac{1}{n} \ln C_e \quad (5)$$

The Langmuir plot (Figure 5) showed excellent linearity (R^2 = 0.998), indicating monolayer adsorption on a homogeneous population of binding sites and yielding a monolayer capacity (qmax) of 69.4 mg g^{-1}. This behavior is consistent with the uniform distribution of AB193 ligands introduced through diazonium grafting.

The Freundlich model exhibited a lower correlation (R^2 = 0.888), suggesting limited surface heterogeneity and confirming that multilayer adsorption is not a major contributor to the sorption process. The Langmuir capacity significantly exceeds those reported for AB193 immobilized on XAD-4 (20.9 mg g^{-1}) [31] and XAD-2 (3.35 mg g^{-1}) [32], as summarized in Table 2, demonstrating the influence of mesoporosity, high surface area and enhanced ligand exposure in improving metal uptake.

The isotherm plots in Figure 5 demonstrate that the Langmuir model (qmax = 68.6 mgg^{-1}, KL = 0.1 L/mg, R^2 = 0.998) aligns more closely with experimental data than the Freundlich model (KF = 27.88, n = 4.9, R^2 = 0.888). This indicates that chemisorption, driven by uniform active sites, is the dominant mechanism. The application of both models not only confirms the adsorption mechanism but also underscores the Langmuir model's superior predictive accuracy. Consequently, this supports its use in designing efficient solid phase extraction (SPE) sorbent materials, particularly mesoporous nanomaterials, which provide high surface areas and consistent binding sites

3.2.4. Eluent strength and desorption efficiency

Desorption behavior was investigated using HNO_3 solutions of varying concentration (Figure 6). Recovery increased progressively from ~15% at 0.25 M HNO_3 to ~76% at 0.5 M, reflecting partial protonation of ligand donor groups. Quantitative desorption (~99%) was achieved at 1.0 M HNO_3, beyond which no further improvement was observed. This outcome reflects the proton-sensitive nature of Cr(III)–ligand coordination, indicating that 1.0 M HNO_3 provides the minimum acidity required for complete ligand protonation and full release of Cr(III) while maintaining structural stability of the sorbent.

Optimizing eluent strength is essential for ensuring quantitative recovery, preventing analyte carryover, and supporting long-term sorbent reusability. These observations complete the evaluation of the uptake–release cycle and form the basis for a mechanistic synthesis presented in Section 3.2.5.

3.2.5. Mechanism of Cr(III) uptake

Integration of the pH-dependent adsorption behavior, kinetic modelling, equilibrium isotherms and desorption characteristics (Figures 3-6) reveals a coherent mechanistic framework governing Cr(III) uptake on MSNs–AB193. [33] Maximum adsorption at pH 5 corresponds to optimal ligand deprotonation and favorable Cr(III) speciation, enabling efficient coordination at azo–phenolic donor sites. The strong conformity to the pseudo-second-order model indicates chemisorption as the dominant interaction, while the Langmuir fit confirms that adsorption occurs on a homogeneous array of binding sites formed through uniform diazonium grafting.

The effective desorption with 1.0 M HNO_3 supports a mechanism driven by proton-sensitive complexation. Comparison with the markedly lower sorption capacities of AB193-modified XAD resins (Table 2) emphasizes the contributions of mesoporosity, high ligand accessibility and surface uniformity in enhancing uptake. Collectively, these findings provide the mechanistic basis for the operational parameters employed in the optimized dSPE procedure.

3.3. Analytical performance of the optimized dSPE–ICP-MS procedure

The calibration of Cr(III) in groundwater a matrix showed excellent linearity (R^2 ≥ 0.993) and low LODs (≤0.009 μg/L), confirming

Table 3. Calibration parameters for Cr(III) ions following dSPE using MSNs-AB193.

Calibration parameter	Cr (III)
Concentration range (μgL^{-1})	Blank-50
Calibration coefficient R^2	0.998
RSD at 5 ngmL^{-1} (%n=3) RSD at 85 ngmL^{-1} (%n=3)	1.73 2.34
Sensitivity, CPS ratio/(μgL^{-1})	2.21
LOD (μg/L)	0.007

Table 4. Analysis of Cr (III) in groundwater (ES-L-1) materials after dSPE using AB193-MSNs (values expressed as mean ± RSD in μg·L^{-1} and recovery %).

Groundwater (ES-L-1)	Values
Certified	20*
Found	19.7±0.01
Recovery %	95

* 20 μg·L^{-1} tabulated in certificate as 0.02 mg/l

the method's suitability for the detection of Cr (III) ion at trace concentrations. Precision was acceptable (<3.1% RSD), though slightly lower in wastewater, reflecting higher matrix complexity. Sensitivity values were relatively comparable, demonstrating the robustness of MSNs-AB193 sorbent for dSPE across different matrices (Table 3).

The accuracy of the developed dSPE analytical method employing AB193-MSNs as a chelating sorbent was confirmed using certified wastewater (EU-L-1) and groundwater (ES-L-1) reference materials (CRM). The CRM samples were processed following the same dSPE protocol described in the experimental part. The measured concentrations (0.14 ± 0.01 and 0.019 ± 0.01 μg·L^{-1}, respectively) were in close agreement with the certified values (0.15 and 0.020 μg·L^{-1}), corresponding to recoveries of 93–95% (Table 4).

3.4. Interference studies

Although AB193 possesses intrinsic coordination sites with high affinity for Cr(III), thiourea was additionally employed as a masking agent to suppress competitive complexation by coexisting transition metals such as Fe^{3+}, Cu^{2+}, Ni^{2+}, Mn^{2+}, Zn^{2+}, and Pb^{2+}—a strategy consistent with the masking approach described by Ameer and Hussain [22]. This combined chelation–masking mechanism significantly enhances the overall selectivity of Cr(III) in multi-ion matrices.

The interference results (Table S1 in supplementary) show that abundant alkali and alkaline-earth ions (Na^+, K^+, Mg^{2+}, Ca^{2+}), as well as several transition metals present at concentrations 60–100 times higher than Cr(III), exert minimal influence on the dSPE performance. Cr(III) recoveries consistently remained within 94–98%, demonstrating that MSNs–AB193 preserves strong selectivity and quantitative extraction capacity even under elevated ionic-strength conditions. This high tolerance toward competitive ions confirms the suitability of the sorbent for natural groundwater and moderately contaminated wastewater samples

3.5. Application to real samples

The validated MSNs–AB193-based dSPE method was successfully applied to groundwater samples collected from the Al-Madinah Al-Munawarah region, Saudi Arabia. Ascorbic acid was added before extraction to reduce Cr(VI) quantitatively to Cr(III), following established protocols [34]. This reduction step ensures complete capture of all inorganic chromium species as Cr(III) by the functionalized sorbent and enables accurate determination of total chromium.

Groundwater samples without spiking contained total chromium concentrations between 13.74 and 17.0 μg·L^{-1}, well below the World Health Organization (WHO) guideline value of 50 μg·L^{-1} for total chromium in drinking water [35] (Table 5). Samples spiked at the 10 μg·L^{-1} level showed recoveries of 92.2–99.4%, demonstrating negligible matrix interference and confirming the method's reliability for routine

Table 5. Chromium analysis from real groundwater and wastewater sample and WHO limit comparison.

Sample	Added (μg·L^{-1})	Found (μg·L^{-1})	Recovery (%)	WHO limit (μg·L^{-1})
GW1	--	15.32	--	
GW1	10	24.54	92.20	50
GW2	---	17.0		
GW2	10	26.68	96.8	50
GW3	--	14.35		
GW3	10	24.29	99.4	50
GW4	--	13.74		
GW4	10	23.43	96.9	50

environmental monitoring. These consistently high recoveries further confirm that AB193-functionalized MSNs maintain strong and selective Cr(III) binding affinity in complex real-world matrices.

3.6. Resin reusability and stability

The MSNs–AB193 sorbent demonstrated strong chemical durability across a wide range of conditions. Exposure to acidic media up to 3 M HNO_3 did not induce detectable structural degradation, consistent with the robustness associated with aryl diazonium-derived surface linkages [19,20]. Under mildly alkaline conditions (up to 3 M NH_4OH), only a minor decrease in sorption capacity (~2.3%) was observed, likely due to partial silica dissolution and slight chromophore alteration, effects commonly reported for mesoporous silica at elevated pH [10,20].

The assessment of operational reusability showed that the same batch of material retained its performance over ten consecutive sorption–desorption cycles (Figure 7). The overall reduction in sorption capacity remained below 2.5%, indicating excellent regeneration efficiency and minimal functional-group degradation throughout repeated use. Long-term storage stability was also confirmed, with no measurable decline in extraction efficiency after more than ten months of storage in a desiccator. These findings collectively demonstrate that MSNs–AB193 possesses the necessary chemical and operational stability for routine analytical applications, including repeated extraction cycles and extended storage periods.

4. Conclusions

This study introduces the first successful application of aryl diazonium chemistry for the covalent immobilization of a Cr(III)-selective azo dye, Acid Blue 193, onto MSNs. The obtained hybrid nanochelator, MSNs–AB193, combines the exceptional stability of diazonium-derived C–Si/C–O linkages with the high surface area and ordered porosity of MSNs, delivering a robust, selective, and high-capacity sorbent for trace chromium (III). When integrated into an optimized dispersive solid-phase extraction protocol with ICP-MS detection, the sorbent enables accurate and sensitive determination of total inorganic chromium in environmental waters, as demonstrated by excellent recoveries from certified reference materials and real groundwater samples from Al-Madinah Al-Munawarah. The combination of ascorbic acid reduction of Cr(VI) to Cr(III) and thiourea masking of competing ions ensures reliable speciation-independent measurement even in the presence of complex matrices. The high sorption capacity of ~68 mg·g^{-1}, fast chemisorption kinetics, quantitative elution with dilute nitric acid, and proven reusability over multiple cycles, together with exceptional long-term storage stability, highlight the practical robustness of the material. These attributes extend its utility far beyond trace analysis. Simple scaling of sorbent quantity and sample volume allows direct adaptation of MSNs–AB193 for efficient removal and subsequent recovery of chromium from chromium-rich industrial effluents, including tannery, electroplating, and textile wastewaters. This dual capability-ultra-trace monitoring and preparative-scale remediation with potential metal recovery-positions the developed nanochelator as a versatile and sustainable tool for both environmental protection and resource valorization.

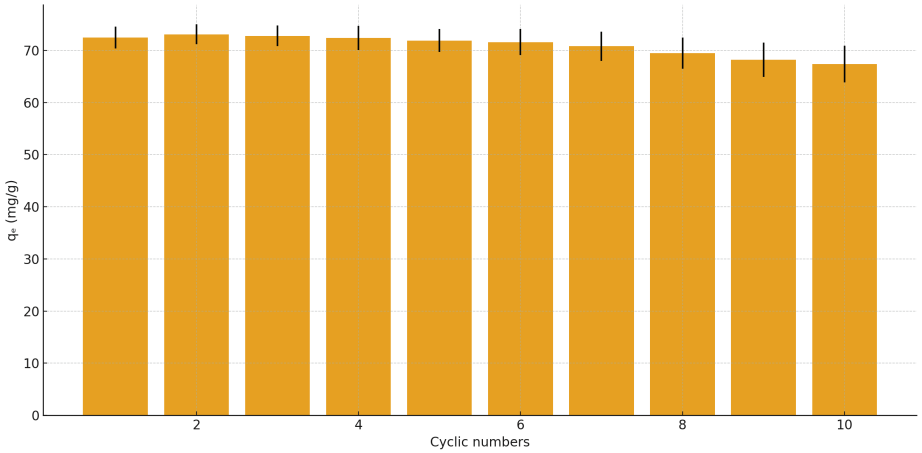

Figure 7. Reusability of MSNs–AB193 nanochelator over ten cycles, showing a capacity loss of less than 2.5 %.

CRediT authorship contribution statement

The author solely contributed to the conception, design, experimental work, data analysis, manuscript preparation, and final approval.

Declaration of competing interest

There are no conflicts of interest.

Declaration of generative AI and AI-assisted technologies in the writing process

The author confirms the use of generative artificial intelligence (ChatGPT, OpenAI) to enhance the readability and clarity of some parts of the manuscript. The author takes full responsibility for the content of the manuscript.

Acknowledgment

The author is grateful to the Department of Chemistry at Taibah University for providing the necessary facilities to carry out this work.

Supplementary data

Supplementary material to this article can be found online at https://dx.doi.org/10.25259/AJC_1051_2025.

References

1. Camel, V., 2003. Solid phase extraction of trace elements. *Spectrochimica Acta Part B: Atomic Spectroscopy*, **58**, 1177-1233. https://doi.org/10.1016/s0584-8547(03)00072-7
2. Chisvert, A., Cárdenas, S., Lucena, R., 2019. Dispersive micro-solid phase extraction. *TrAC Trends in Analytical Chemistry*, **112**, 226-233. https://doi.org/10.1016/j.trac.2018.12.005
3. Ścigalski, P., Kosobucki, P., 2020. Recent materials developed for dispersive solid phase extraction. *Molecules (Basel, Switzerland)*, **25**, 4869. https://doi.org/10.3390/molecules25214869
4. Barani, S.; Sebastian, S. P.; Dhevagi, P.; Prasanthrajan, M.; Suganthi, A., 2024. Synthesis of silica nanoparticles (SiNPs) from agro-wastes for removal of heavy metals from an aqueous medium – a mini review. *Green Chemistry Letters and Reviews* **17,** 2422416. https://doi.org/10.1080/17518253.2024.2422416.
5. Dorairaj, D., Govender, N., Zakaria, S., Wickneswari, R., 2022. Green synthesis and characterization of UKMRC-8 rice husk-derived mesoporous silica nanoparticle for agricultural application. *Scientific Reports*, **12**, 20162. https://doi.org/10.1038/s41598-022-24484-z
6. Yan, X., Meng, J., Hu, X., Feng, R., Zhou, M., 2019. Synthesis of thiol-functionalized mesoporous silica nanoparticles for adsorption of Hg^{2+} from aqueous solution. *Journal of Sol-Gel Science and Technology*, **89**, 617-622. https://doi.org/10.1007/s10971-019-04923-6
7. Yu, J., Bondarieva, A., Pylypenko, I., Tobilko, V., Sabov, T., Gumenna, M., Tomila, T., Inshyna, O., 2025. Amino-functionalized dendritic mesoporous silica nanoparticles for removal of copper from aqueous solutions. *Journal of Ecological Engineering*, **26**, 365-377. https://doi.org/10.12911/22998993/202979
8. Saadat, A., Bnaei, A., Seyedyosefi, F., Pargol Ghasemi, P., 2022. Preparation of silica-coated magnetite nanoparticles with thiophosphoramide for removal of heavy metals from aqueous solutions, Iran. *Journal of Chemical Engineering*, **42**, 916-924. https://doi.org/10.30492/ijcce.2022.547124.5129.
9. Al-Wasidi, A.S., Katouah, H.A., Saad, F.A., Abdelrahman, E.A., 2023. Functionalization of silica nanoparticles by 5-chloro-8-quinolinol as a new nanocomposite for the efficient removal and preconcentration of Al^{3+} ions from water samples. *ACS Omega*, **8**, 15276-15287. https://doi.org/10.1021/acsomega.3c00413
10. AlMohaimadi, K.M., Albishri, H.M., Althumayri, K., AlSuhaimi, A.O., Hussein, B.H.M., 2025. Preparation of phenanthroline-2-carbaldehyde functionalized mesoporous silica nanoparticles as nanochelator for solid phase extraction of trace metals from wastewater. *Arabian Journal of Chemistry*, **18**, 792024. https://doi.org/10.25259/ajc_79_2024
11. Li, W., Xu, Y., Zhou, Y., Ma, W., Wang, S., Dai, Y., 2012. Silica nanoparticles functionalized via click chemistry and ATRP for enrichment of Pb(II) ion. *Nanoscale Research Letters*, **7**, 485. https://doi.org/10.1186/1556-276X-7-485
12. del Campo, A., Sen, T., Lellouche, J.P., Bruce, I.J., 2005. Multifunctional magnetite and silica–magnetite nanoparticles: Synthesis, surface activation and applications in life sciences. *Journal of Magnetism and Magnetic Materials*, **293**, 33-40. https://doi.org/10.1016/j.jmmm.2005.01.040
13. Zhu, M., Lerum, M.Z., Chen, W., 2012. How to prepare reproducible, homogeneous, and hydrolytically stable aminosilane-derived layers on silica. *Langmuir : The ACS Journal of Surfaces and Colloids*, **28**, 416-423. https://doi.org/10.1021/la203638g
14. Gam-Derouich, S., Mahouche-Chergui, S., Turmine, M., Piquemal, J.Y., Hassen-Chehimi, D.B., Omastová, M., Chehimi, M.M., 2011. A versatile route for surface modification of carbon, metals and semi-conductors by diazonium salt-initiated photopolymerization. *Surface Science*, **605**, 1889-1899. https://doi.org/10.1016/j.susc.2011.06.029
15. Griffete, N., Ahmad, R., Benmehdi, H., Lamouri, A., Decorse, P., Mangeney, C., 2013. Elaboration of hybrid silica particles using a diazonium salt chemistry approach. *Colloids and Surfaces A: Physicochemical and Engineering Aspects*, **439**, 145-150. https://doi.org/10.1016/j.colsurfa.2013.03.071
16. Sandomierski, M., Strzemiecka, B., Chehimi, M.M., Voelkel, A., 2016. Reactive diazonium-modified silica fillers for high-performance polymers. *Langmuir: The ACS Journal of Surfaces and Colloids*, **32**, 11646-11654. https://doi.org/10.1021/acs.langmuir.6b02891
17. Hetemi, D., Noël, V., Pinson, J., 2020. Grafting of diazonium salts on surfaces: Application to biosensors. *Biosensors*, **10**, 4. https://doi.org/10.3390/bios10010004
18. Sandomierski, M., Voelkel, A., 2021. Diazonium modification of inorganic and organic fillers for the design of robust composites: A review. *Journal of Inorganic and Organometallic Polymers and Materials*, **31**, 1-21. https://doi.org/10.1007/s10904-020-01725-0
19. AlQadhi, N.F., AlSuhaimi, A.O., 2020. Chemically functionalized activated carbon with 8-hydroxyquinoline using aryldiazonium salts/diazotization route: Green chemistry synthesis for oxins-carbon chelators. *Arabian Journal of Chemistry*, **13**, 1386-1396. https://doi.org/10.1016/j.arabjc.2017.11.010
20. AlSuhaimi, A.O., 2025. Amberlite XAD-4 functionalized with 4-(2-Pyridylazo) resorcinol via aryldiazonium chemistry for efficient solid-phase extraction of trace metals from groundwater samples, *Applied Sciences*, **15**, 9044. https://doi.org/10.3390/app15169044.
21. G.K. Zoorob, S. Rashad, N.A. El Zawawy, 2012. Chromium speciation in commercial dyes, by HPLC–CP-MS, *Environmental Toxicology and Chemistry*, **31** 1240–1246. https://doi.org/10.1002/etc.1829.
22. Ameer, A. H. A. H.; Hussain, A. F., 2023. Spectrophotometric determination of micro chromium(III) using an azo dye ligand: masking and analytical applications. *Baghdad Science Journal* **20** (2023) 1331–1341. https://doi.org/10.21123/bsj.2023.7393.
23. Malki, M.; AlSuhaimi, A. O.; AlSehli, B. R.; AlMohaimadi, K. M.; AlThumairy, K. A.; AlMohdar, Y.; AlHarbi, S.; Heisen, B., 2026. Sustainable room-temperature sol–gel synthesis of mesoporous silica nanoparticles from sodium silicate using ascorbic acid and nonionic *Surfactants for Amoxicillin Removal from Water*. RSC Advances (submitted).

24. Qafoku, N.P., Lawter, A.R., Shao, H., Wang, G., Brown, C.F., 2014. Evaluating impacts of CO_2 gas intrusion into a confined sandstone aquifer: Experimental results. *Energy Procedia*, **63**, 3275-3284. https://doi.org/10.1016/j.egypro.2014.11.355
25. Quinton, D., Galtayries, A., Prima, F., Griveau, S., 2012. Functionalization of titanium surfaces with a simple electrochemical strategy. *Surface and Coatings Technology*, **206**, 2302-2307. https://doi.org/10.1016/j.surfcoat.2011.10.008
26. Socrates, G., 2010. Infrared and Raman characteristic group frequencies: Tables and charts, 3. ed., repr. as paperback, Wiley, Chichester, 2010. pp 230-235.
27. Żmijewski, T., Mioduska, M., Pacewska, B., 1987. Thermogravimetric study of silica with a chemically modified surface. *Journal of Thermal Analysis*, **32**, 1755-1761. https://doi.org/10.1007/bf01913962
28. Shams Jalbani, N., Solangi, A.R., Memon, S., Junejo, R., Ali Bhatti, A., Lütfi Yola, M., Tawalbeh, M., Karimi-Maleh, H., 2021. Synthesis of new functionalized Calix[4]arene modified silica resin for the adsorption of metal ions: Equilibrium, thermodynamic and kinetic modeling studies. *Journal of Molecular Liquids*, **339**, 116741. https://doi.org/10.1016/j.molliq.2021.116741
29. Thommes, M., Kaneko, K., Neimark, A.V., Olivier, J.P., Rodriguez-Reinoso, F., Rouquerol, J., Sing, K.S.W., 2015. Physisorption of gases, with special reference to the evaluation of surface area and pore size distribution (IUPAC Technical Report). *Pure and Applied Chemistry*, **87**, 1051-1069. https://doi.org/10.1515/pac-2014-1117
30. Zhang, N., Bao, J., Bai, X., Yuan, L., 2008. Chromium(III)-imprinted silica gel for speciation analysis of chromium in water. *Analytica Chimica Acta*, **613**, 119-126. https://doi.org/10.1016/j.aca.2008.04.047.
31. Marin, N. M. Adsorption of heavy metals onto amberlite xad 4 resin chelated with acid blue 193. In: Book of Abstracts SIMI 2023, National Research and Development Institute for Industrial Ecology, *Bucharest*, pp. 14–15. https://doi.org/10.21698/simi.2023.ab01.
32. Marin, N. M. Adsorption of Cr^{3+}, Cu^{2+} and Fe^{3+} onto amberlite xad 2 resin functionalized with acid blue 193. In: Book of Abstracts SIMI 2022, National Research and Development Institute for Industrial Ecology, *Bucharest*, pp. 16–17. https://doi.org/10.21698/simi.2022.ab01.
33. Weber, W. J.; Morris, J. C. Kinetics of adsorption on carbon from solution. *Journal of the Sanitary Engineering Division* **89** (2) (1963) 31–59. https://doi.org/10.1061/JSEDAI.0000430.
34. Saad, E. M.; Butler, I. S.; Mostafa, S. I. Adsorption of reduced chromium(VI) ions by vitamin C tablets onto a tellurato-functionalized cellulose derivative and its composite with Cyanobacteria green algae in aqueous media. *Environmental Progress & Sustainable Energy* **40** (2021) e13608. https://doi.org/10.1002/ep.13608.
35. World Health Organization. Guidelines for drinking-water quality: fourth edition incorporating first addendum, 4th ed., 1st add. World Health Organization, Geneva, 2017.